Available online at www.sciencedirect.com
ScienceDirect
Trans. Nonferrous Met. Soc. China 32(2022) 3679−3686
Transactions of Nonferrous Metals Society of China
www.tnmsc.cn

Lithium-ion diffusion path of tetragonal tungsten bronze (TTB) phase $Nb_{18}W_{16}O_{93}$

Chao SHEN[1,2], Sai-nan JIANG[1], Cui-min DING[1], Wei-shun XUE[3], Ke-yu XIE[1,2]

1. State Key Laboratory of Solidification Processing, Center for Nano Energy Materials, School of Materials Science and Engineering, Northwestern Polytechnical University, Xi'an 710072, China;
2. Research & Development Institute of Northwestern Polytechnical University in Shenzhen, Northwestern Polytechnical University, Shenzhen 518057, China;
3. Tianjin Institute of Power Sources, Tianjin 300384, China

Received 22 September 2021; accepted 6 April 2022

Abstract: By taking tetragonal tungsten bronze (TTB) phase $Nb_{18}W_{16}O_{93}$ as an example, an improved solid-state sintering method at lower temperature of 1000 °C for 36 h was proposed via applying nanoscale raw materials. XRD, SEM and XPS confirm that the expected sample was produced. GITT results show that the lithium-ion diffusion coefficient of $Nb_{18}W_{16}O_{93}$ (10^{-12} cm^2/s) is higher than that of the conventional titanium-based anode, ensuring a relatively superior electrochemical performance. The lithium-ion diffusion mechanism was thoroughly revealed by using density functional theory simulation. There are three diffusion paths in TTB phase, among which the interlayer diffusion with the smallest diffusion barrier (0.46 eV) has more advantages than other typical anodes (such as graphite, 0.56 eV). The relatively smaller lithium-ion diffusion barrier makes TTB phase $Nb_{18}W_{16}O_{93}$ become a potential high-specific-power anode material.

Key words: lithium-ion battery; niobium tungsten oxide; tetragonal tungsten bronze (TTB) phase; lithium-ion diffusion mechanism; diffusion path

1 Introduction

With the rising demand for high power and fast charging electric equipment, developing high-rate lithium-ion batteries is urgent [1]. Graphite is one of the tradition anodes, with a high theoretical capacity (372 mA·h/g) [2]. When graphite anode was charged at a high rate, phase transition often occurred, causing volume change. Through the accurate multielement chemical substitution engineering, XIAO et al [3] inhibited the phase transformation during the cycle and prepared the cathode with high structural reversibility. Regulating phase transition [4] is also a strategy for improving anode performance. However, to expand the further application of lithium-ion batteries, anode materials with higher rates and safety must be pursued.

Niobium tungsten oxides refer to a series of Nb_2O_5−WO_3 binary oxides and belong to lithium-ion intercalation/deintercalation materials [5]. They have a unique 3D-structure lithium-ion transmission channel, which is conducive to the rapid spread of lithium-ion [6], with remarkable lithium-ion diffusion rate and superior rate performance [7,8]. Niobium tungsten oxides are mainly divided into two structures: Wadsley−Roth phase [9] and tetragonal tungsten bronze (TTB) phase [5,7,10−13]. As early as 1968, STEPHENSON [14] found several niobium tungsten oxides (such as $Nb_{18}W_{16}O_{93}$) that belong to the TTB phase. The

Corresponding author: Chao SHEN, Tel: +86-17792394585, Fax: +86-28-88460308, E-mail: shenchao@nwpu.edu.cn
DOI: 10.1016/S1003-6326(22)66048-5

TTB phase is composed of pentagonal units surrounded by metal oxygen octahedra. The units are connected to one another to form a pentagonal tunnel, providing a fast channel for lithium-ion transmission [15]. However, the performance of using TTB phase material as anode for lithium-ion batteries is still unclear [16−18]. In 2018, the performance of the micron-sized niobium tungsten oxide was studied by GRIFFITH et al [19]. The traditional nanostructure strategy leads to the reduction of volume energy density and safety. Instead, the micron-size $Nb_{16}W_5O_{55}$ and $Nb_{18}W_{16}O_{93}$ were found to have excellent rate performance and volume energy density [20].

More researches were conducted on the Wadsley−Roth phase (such as $Nb_{14}W_3O_{44}$), but the structure and working mechanism of TTB phase remain puzzling. In the existing literature, the conditions for preparing niobium tungsten oxide are very strict. The preparation of niobium tungsten oxide reported by ROTH and WADSLEY [21] requires sintering at a temperature between 1300 and 1400 °C for 24−72 h. The long-term high-temperature sintering preparation method consumes time and cost, and potential safety hazards exist in large-scale production.

Herein, an improved solid-state sintering synthesis method was introduced, and the electrochemical performance and lithium-ion diffusion kinetic parameters of TTB phase $Nb_{18}W_{16}O_{93}$ were studied. Nano-scale Nb_2O_5 and WO_3 were used as raw materials, and $Nb_{18}W_{16}O_{93}$ with expected crystal structure was prepared at 1000 °C which is lower than that in previously-reported literature. The phase structure of the product was characterized by X-ray diffraction (XRD), X-ray photoelectron spectrometer (XPS) and scanning electron microscopy (SEM). In addition, the as-prepared $Nb_{18}W_{16}O_{93}$ was used as an anode material to assemble a button cell, and its electrochemical performance was studied. To obtain deep insights into the role of 3D tunnel network of $Nb_{18}W_{16}O_{93}$, rating performance testing and theoretical calculation were carried out to reveal the internal ion diffusion mechanism.

2 Experimental

2.1 Sample preparation and characterizations

Nano Nb_2O_5 and nano WO_3 powders with a Nb/W stoichiometric ratio of 18:16 were thoroughly ground and mixed in a mortar for 10 min. Then, the resulting mixture was transferred to a corundum porcelain boat, sintered in a muffle furnace at 1000 °C for 36 h and cooled to room temperature in the furnace after heating. In the experiment, the use of nano powder as raw material, compared with the methods mentioned in the previous literature, reduced sintering temperature and time, and saved energy.

The as-prepared products were characterized and analyzed by using XRD spectroscopy (Xpert Pro MPD), SEM (FEI NANO450), and XPS (ESCALAB 250Xi).

All calculations were performed within the framework of the density functional theory, as implemented in the Vienna Ab initio Software Package (VASP 5.3.5) code within the Perdew–Burke–Ernzerhof generalized gradient approximation and the projected augmented wave method [22−25]. The cut-off energy for the plane wave basis set was set to be 450 eV. The Brillouin zone of the surface unit cell was sampled by Monkhorst–Pack grids for $Nb_{18}W_{16}O_{93}$ structure optimalisation [26]. The $Nb_{18}W_{16}O_{93}$ structure was determined by 1×1×2 Monkhorst−Pack grid. The convergence criterion for the electronic self-consistent iteration and force were set to be 10−5 eV and 0.01 eV/Å, respectively. The climbing image nudged elastic band [27−29] method was used to confirm the transition states with only one imaginary frequency along the reaction coordinates.

2.2 Electrochemical tests

To verify the rating performance and power density of $Nb_{18}W_{16}O_{93}$ anode electrode, the prepared product was uniformly mixed with conductive carbon black and PVDF according to a mass ratio of 8:1:1, and an appropriate amount of NMP was added to grind fully and mix into a negative electrode slurry with a suitable viscosity. The slurry on the copper foil was coated using a spatula and dried in a blast drying oven until the surface was dry. Then, the copper foil was transferred to a vacuum drying oven and vacuum dried at 80 °C for 6 h. Finally, the dried negative electrode sheet was punched into a disc with 12 mm in diameter, which was weighed for later use.

In a glove box with an argon atmosphere, the electrode sheet, separator, electrolyte, lithium sheet,

positive and negative battery shells and gaskets were assembled into a CR2016 button cell. After the assembly was completed, it stood for 12 h for electrochemical performance test. The cycle performance, galvanostatic intermittent fraction technique (GITT), dQ/dV and rate performance were carried out using a LAND battery test instrument.

3 Results and discussion

3.1 Morphology and structure

The prepared material was tested by XRD to investigate the crystal structure. Figure 1(a) calibrates the XRD diffraction spectrum of $Nb_{18}W_{16}O_{93}$. Figure 1(a) shows that the XRD diffraction peaks are sharp, indicating that it has good crystallinity. The main diffraction peaks of the material are consistent with $Nb_{18}W_{16}O_{93}$ (JCPDS No.75-0561), which are located at 16.244°, 22.588°, 23.032°, 26.312°, 30.195°, 32.818°, 34.962°, 38.045°, 47.101° and 53.041° and can be calibrated as (160), (001), (021), (290), (430), (460), (291), (431), (571) and (730) crystal planes, respectively. This structure belongs to the TTB phase structure, monoclinic system and *Pbam* space group. The basic unit of the TTB phase is a pentagonal structure surrounded by metal oxygen tetrahedrons. This pentagonal structure is stacked in a 3D space to form a pentagonal channel. Thus, the material has an excellent lithium-ion diffusion superiority. XRD image analysis shows that the improved solid-phase sintering method used in the experiment can successfully synthesize $Nb_{18}W_{16}O_{93}$ at a lower temperature.

In 1968, STEPHENSON [14] studied several niobium tungsten oxides (such as $Nb_{18}W_{16}O_{93}$) with a different structure (TTB phase). Figure 1(b) shows that this phase is composed of pentagonal units surrounded by metal oxygen octahedra. The units are connected to one another to form a pentagonal tunnel. This structure provides a fast channel for lithium-ion diffusion.

To characterize the element composition and valence state of micron $Nb_{18}W_{16}O_{93}$, an XPS test was performed, as shown in Fig. 2. The XPS full spectrum of Fig. 2(a) shows that Nb, W and O elements coexist in the sample. Figures 2(c, d) show the enlarged fine spectra of Nb 3d and W 4f, respectively. The two peaks of Nb 3d at 207.17 and 209.97 eV in Fig. 2(c) can be ascribed to the Nb $3d_{5/2}$ splitting peak and the Nb $3d_{3/2}$ splitting peak, respectively, which proves that the Nb element in the sample exists in the form of Nb^{5+}. The two peaks of W 4f at 35.77 and 37.87 eV in Fig. 2(d) can be attributed to the W $4f_{7/2}$ splitting peak and the W $4f_{5/2}$ splitting peak, respectively, which proves that the W element in the sample exists in the form of W^{6+}. The XPS results further confirm that the product belongs to the Nb_2O_5−WO_3 series of oxides. Figure 2(b) shows that $Nb_{18}W_{16}O_{93}$ is agglomerated from approximately 2 μm-long and 600 nm-diameter rod-shaped crystal grains into secondary particles with a particle size of approximately 5 μm.

3.2 Lithium-ion diffusion path

The first-principle calculations [28,30] were conducted to understand the influencing effect of the $Nb_{18}W_{16}O_{93}$ 3D open tunnel network in improving the lithium-ion diffusion capacity. The result in Fig. 3(a) shows that $Nb_{18}W_{16}O_{93}$ presents a layered structure with numerous interconnected

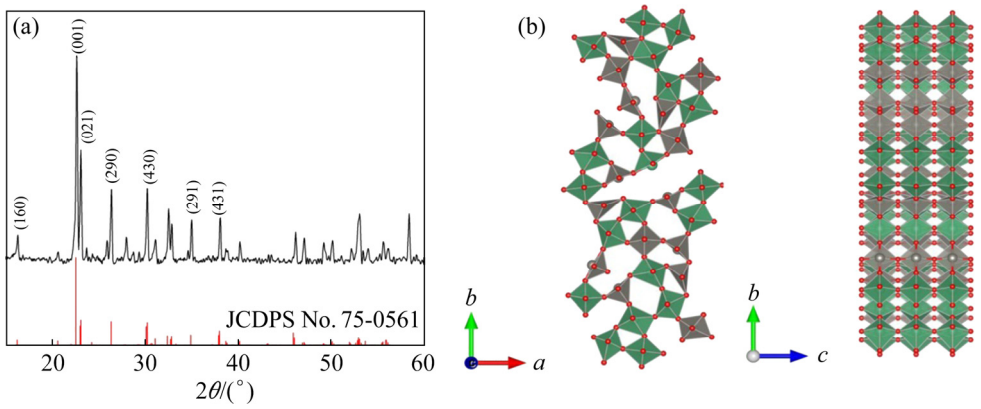

Fig. 1 XRD patterns (a) and crystal structure (b) of $Nb_{18}W_{16}O_{93}$ (The red circles represent the O atoms, the green circles stand for Nb atoms and the grey circles stand for W atoms)

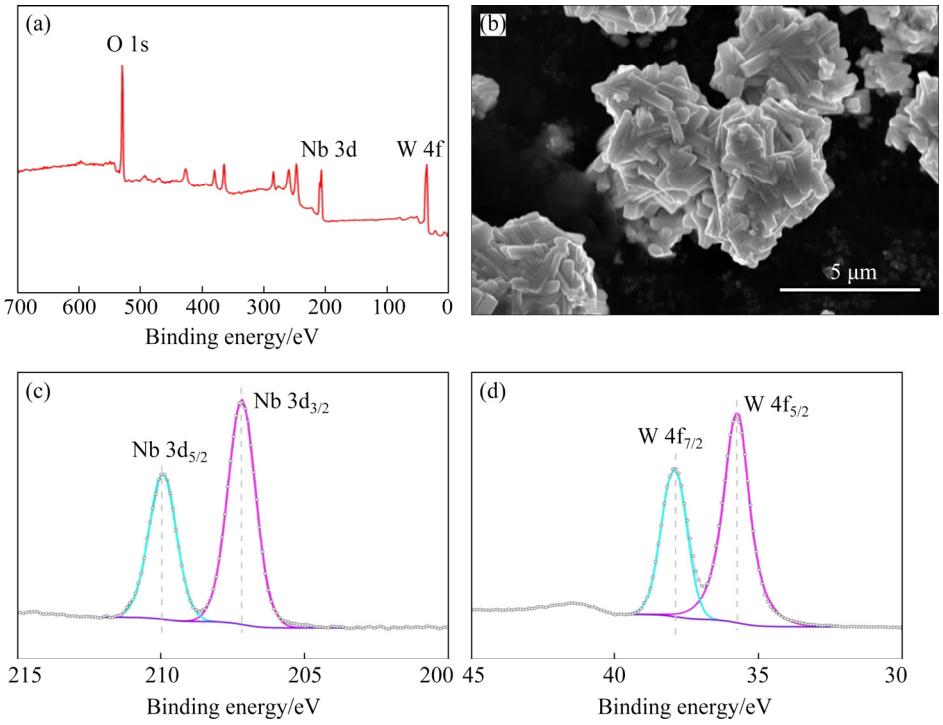

Fig. 2 XPS pattern (a), SEM image (b), Nb 3d XPS spectra (c) and W 4f XPS spectra (d) of $Nb_{18}W_{16}O_{93}$

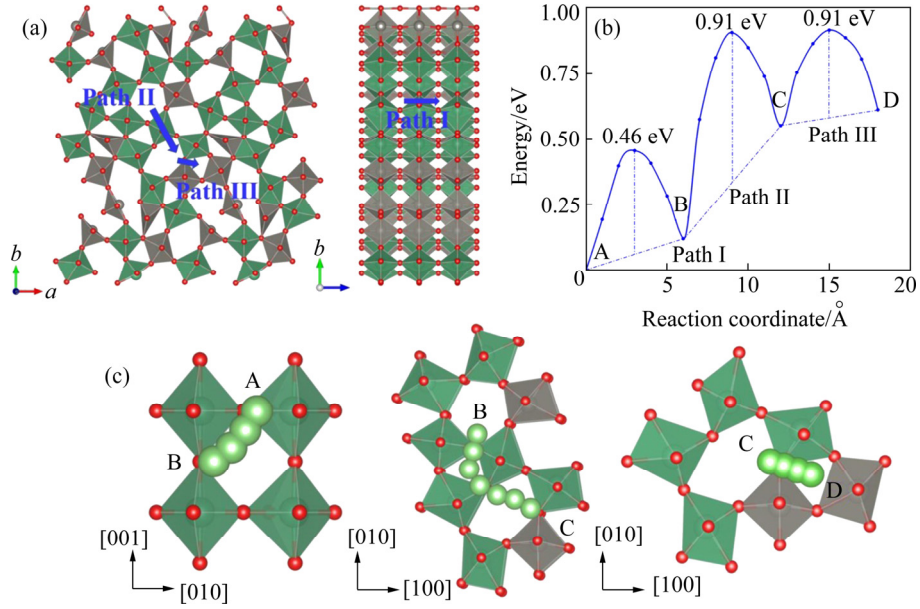

Fig. 3 Lithium-ion diffusion path (a), diffusion energy barriers corresponding to different paths (b); start and end points of lithium-ion movement in different paths (c) (The red circles represent the O atoms, the green circles stand for Nb atoms and the grey circles stand for W atoms)

tunnel structure holes on the surface. The layered structure of $Nb_{18}W_{16}O_{93}$ provides an infinite number of lithium diffusion 2D channels, such as channels in the *a*–*b* crystallographic plane. Additional pentagonal channels (along the *c* axis) provide 3D paths for the long-distance diffusion of lithium ions.

$Nb_{18}W_{16}O_{93}$ has three main lithium-ion diffusion channels, namely, interlayer diffusion Path I and intralayer diffusion Paths II and III. The mobility behavior of lithium ions in different transmission paths depends on the diffusion energy barrier on the path. In this work, theoretical calculations are used to obtain the diffusion barriers

of lithium ions on these three diffusion paths. The TTB phase is composed of pentagonal units surrounded by metal oxygen octahedra, and the units are connected to one another to form a pentagonal tunnel. Path I is interlayer diffusion, starting at Point A and ending at Point B. Lithium ions diffuse through the pentagonal tunnel formed by the interconnection of the units in the structure. The diffusion energy barrier is the smallest of the three paths (the minimum energy barrier is 0.46 eV), indicating that the interlayer diffusion is the easiest, because no atoms exist between the layers to hinder its motion and the Path I distance is short. The two remaining types of diffusion, Paths II and III, are intralayer diffusion paths.

Path II starts at Point B and ends at Point C. Path III starts at Point C and ends at Point D. In Path II, after passing through the adjacent triangular channel, lithium ions travel from Point B to Point C that is located in another pentagonal channel. The increase in the energy barrier during the diffusion process is also the largest because the diffusion path of Path II is the longest amongst the three. In Path III, lithium ions diffuse to the adjacent triangular channel D from Point C. Compared with the interlayer diffusion of Path I, Paths II and III are more difficult to accomplish. Paths II and III tend to avoid the metal oxygen octahedron in the path and select the path with the smallest energy barrier for diffusion. However, the pentagonal tunnel, which plays a decisive role in the diffusion of the TTB phase, is more difficult to form. Therefore, compared with the Walsey phase, which is dominated by quadrilateral channel diffusion, the diffusion capacity of the TTB phase is slightly inferior. Meanwhile, the interlayer diffusion energy barrier is smaller than that in common anode materials such as graphite and other anodes, as shown in Table 1, which has the potential to exhibit excellent lithium transport performance.

Table 1 Comparison of theoretically predicted energy barriers for Li^+ diffusion between previously reported anodes and $Nb_{18}W_{16}O_{93}$

Material	Calculated energy barrier for Li^+ diffusion/eV
Graphite	~0.57
$Li_4Ti_5O_{12}$ [10]	0.48−0.7
$Nb_{18}W_{16}O_{93}$	0.46

3.3 Diffusion dynamics

The charge and discharge test of the niobium tungsten oxide electrode material was carried out. The rate performance and cycle performance of $Nb_{18}W_{16}O_{93}$ are shown in Fig. 4. Figure 4(a) shows that the first discharge specific capacity of $Nb_{18}W_{16}O_{93}$ is 186.1 mA·h/g at 1*C*. In terms of rate performance, the discharge specific capacity of $Nb_{18}W_{16}O_{93}$ at a current density of 10*C* is 86.1 mA·h/g, indicating that the rate performance of TTB phase $Nb_{18}W_{16}O_{93}$ is slightly inferior to the Wadsley−Roth phase niobium tungsten oxide recorded in the previous literature. As shown in Fig. 4(d), after 100 cycles, the capacity can maintain at 78.285 mA·h/g. However, due to the larger density of W, resulting in a larger relative molecular mass of $Nb_{18}W_{16}O_{93}$, a higher volume energy density is finally obtained.

Based on the above charge and discharge test results, $Nb_{18}W_{16}O_{93}$ as a lithium-ion battery anode material has good capacity performance and cycle stability, and performs well in high-current charge and discharge.

To explore the redox reversibility and electrochemical reaction mechanism of niobium tungsten oxide, the charge−discharge curve and differential capacitance curve of $Nb_{18}W_{16}O_{93}$ were analyzed, as shown in Fig. 4. Figures 4(b, c) show that $Nb_{18}W_{16}O_{93}$ has multiple reversible reactions in the voltage window of 1.0−3.0 V, amongst which a pair of redox peaks at 2.10/2.15 V correspond to the transition of W^{6+}/W^{5+}, located at the pair of redox peaks at 1.69/1.73 V that corresponds to the transition of Nb^{5+}/Nb^{4+}. The W^{6+}/W^{5+} redox peak of the material is very sharp, because the composition of the material is $Nb_{18}W_{16}O_{93}$, and the proportion of W is larger.

Based on the above analysis of the differential capacitance curve, the charge transfer of the $Nb_{18}W_{16}O_{93}$ material during the charging and discharging process was mainly realized by the reaction of W^{6+}/W^{5+} and Nb^{5+}/Nb^{4+}, whereas the Wadsley−Roth phase niobium tungsten oxide was reported in the previous literature. The charge transfer of Nb^{5+}/Nb^{4+} and Nb^{4+}/Nb^{3+} was mainly realized, which corresponds to the ratio of their Nb and W elements. A material with a larger proportion of W has a higher proportion of W^{6+}/W^{5+} reaction.

Figure 5(a) shows the GITT curve of $Nb_{18}W_{16}O_{93}$ during charging. Figure 5(b) shows the

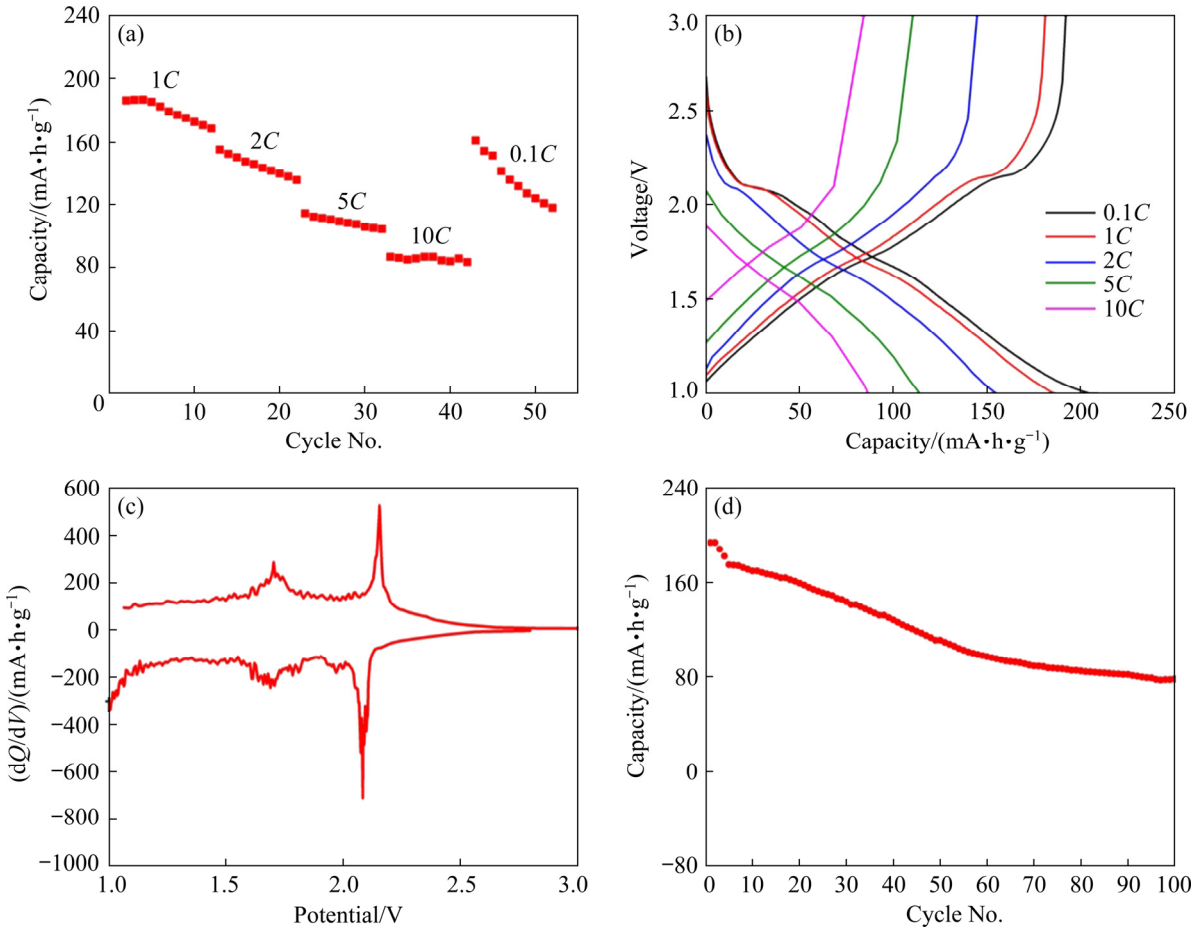

Fig. 4 Rate capabilities (a), galvanostatic discharge−charge curves (b), dQ/dV plots (c), and cycle performance (d) of $Nb_{18}W_{16}O_{93}$

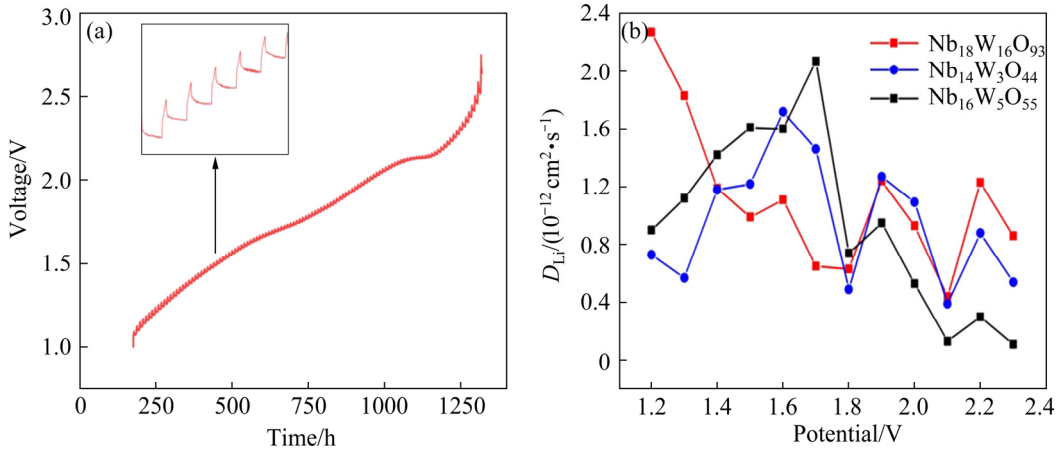

Fig. 5 GITT curve (a) and Li^+ diffusion coefficient (b) of $Nb_{18}W_{16}O_{93}$

lithium-ion diffusion coefficient of the TTB phase $Nb_{18}W_{16}O_{93}$ calculated according to the GITT formula. It is shown that the lithium-ion diffusion coefficients of the two are slightly different, in the order of 10^{-12} cm^2/s, and the lithium-ion diffusion coefficient changing trends with voltage are very similar, which is due to the similar charge and discharge voltage platform of the two phases [3].

4 Conclusions

(1) An improved solid-phase sintering method

with lower temperature and less time was used to prepare TTB phase $Nb_{18}W_{16}O_{93}$. The XRD and XPS results confirm that the expected product is produced. The electrochemical test results show that $Nb_{18}W_{16}O_{93}$ has excellent capacity and rate performance. The GITT test results verify that the lithium-ion diffusion coefficient of $Nb_{18}W_{16}O_{93}$ is about in the order of 10^{-12} cm^2/s, higher than that of the traditional titanium-based anode materials.

(2) Theoretical calculations were carried out to understand the mechanism of the different diffusion paths of lithium ions inside the TTB phase. The results show that the diffusion energy barrier of different paths of $Nb_{18}W_{16}O_{93}$ is small (0.46 eV), which is more beneficial to the lithium ions diffusion. Thus, with excellent electrochemical performance and considerable ions diffusion kinetics, TTB phase $Nb_{18}W_{16}O_{93}$ is a promising anode material for further research and applications.

Acknowledgments

The authors acknowledge the financial support by the Key R&D Program of Shaanxi Province, China (No. 2019ZDLGY04-05), the Natural Science Foundation of Shaanxi Province, China (No. 2019JLZ-01), the Fundamental Research Funds for the Central Universities of China (Nos. 19GH020302, 3102019JC005, 3102021ZD0401, 3102021TS0406), and the Science, Technology, and Innovation Commission of Shenzhen Municipality, China (No. JCYJ20180508151856806).

References

[1] LU Shi-jie, LIU Yang, HE Zhen-jiang, LI Yun-jiao, ZHENG Jun-chao, MAO Jing, DAI Ke-hua. Synthesis and properties of single-crystal Ni-rich cathode materials in Li-ion batteries [J]. Transactions of Nonferrous Metals Society of China, 2021, 31: 1074−1086.

[2] WANG Lu, WANG Zhen-yu, WU Jun-feng, LI Guo-ran, LIU Sheng, GAO Xue-ping. To effectively drive the conversion of sulfur with electroactive niobium tungsten oxide microspheres for lithium−sulfur battery [J]. Nano Energy, 2020, 77: 1−11.

[3] XIAO Yao, WANG Tao, ZHU Yan-fang, HU Hai-yan, TAN Shuang-jie, LI Shi, WANG Peng-fei, ZHANG Wei, NIU Yu-bin, WANG En-hui, GUO Yu-jie, YANG Xin-an, LIU Lin, LIU Yu-mei, LI Hong-liang, GUO Xiao-dong, YIN Ya-xia, GUO Yu-guo. Large-scale synthesis of the stable Co-free layered oxide cathode by the synergetic contribution of multielement chemical substitution for practical sodium-ion battery [J]. Research, 2020: 1469301.

[4] XIAO Yao, ZHU Yan-fang, LI Lin, WANG Peng-fei, ZHANG Wei, LI Chao, DOU Shi-xue, CHOU Shu-lei. Structural insights into the dynamic and controlled multiphase evolution of layered-spinel heterostructured sodium oxide cathode [J]. Cell Reports Physical Science, 2021, 2: 1−12.

[5] MICHAEL W, FRANK K. On the structural complexity of tetragonal tungsten bronze type niobium tungsten oxides [J]. Journal of Inorganic and General Chemistry, 2021, 647: 98−106.

[6] ZHONG Xiao-cong, ZHANG Bin, LIN Zhen-cong, LIU Jia-ming, XIE Yong-min, XU Zhi-feng. Preparation and performance of 3D-Pb anodes for nonferrous metals electrowinning in H2SO4 aqueous solution [J]. Transactions of Nonferrous Metals Society of China, 2020, 30: 535−547.

[7] ANIRUDDHA S L , GUPTA T, SINGH Y, HUNDEKAR P, JAIN R, HAN Fu-dong, KORATKAR N. Aqueous lithium-ion batteries with niobium tungsten oxide anodes for superior volumetric and rate capability [J]. Energy Storage Materials, 2020, 27: 506−513.

[8] TILLEY R J D. The crystal chemistry of the higher tungsten oxides [J]. International Journal of Refractory Metals and Hard Materials, 1995, 13: 93−109.

[9] DONG Sheng-yang, WANG Yi, CHEN Cheng-long, SHEN Lai-fa, ZHANG Xiao-gang. Niobium tungsten oxide in a green water-in-salt electrolyte enables ultra-stable aqueous lithium-ion capacitors [J]. Nano-Micro Letters, 2020, 12: 1−11.

[10] YANG Yang, ZHU He, XIAO Jin-fei, GENG Hong-bo, ZHANG Yu-fei, ZHAO Jin-bao, LI Gen, WANG Xun-li, LI Cheng-chao, LIU Qi. Achieving ultrahigh-rate and high-safety Li^+ storage based on interconnected tunnel structure in micro-size niobium tungsten oxides [J]. Advanced Material, 2020, 32: 1−10.

[11] GAGARINA E, TOPOLOV V, TSIKHOTSKI E, SAKHNENKO V. Multicomponent twins in crystals having structures of the perovskite and the tetragonal tungsten−bronze type [J]. Ferroelectrics, 1992, 126: 335−340.

[12] SARAH K H, DAVID A J. Quaternary lead–niobium–tungsten oxides based on the tetragonal tungsten bronze structure [J]. Journal of Solid State Chemistry, 2001, 161: 135−151.

[13] KIM Y, JACQUET Q, GRIFFITH K J, LEE J, DEY S, RINKEL B L D, GREY C P. High rate lithium ion battery with niobium tungsten oxide anode [J]. Journal of the Electrochemical Society, 2021, 168: 1−8.

[14] STEPHENSON N C. A structural investigation of some stable phases in the region $Nb_2O_5{\cdot}WO_3$−WO_3 [J]. Acta Crystallographica, 1968, B24: 637−653.

[15] KOCER C P, GRIFFITH K J, GREY C P, MORRIS A J. Lithium diffusion in niobium tungsten oxide shear structures [J]. Chemistry of Materials, 2020, 32: 3980−3989.

[16] FRANK K. Order and disorder in niobium tungsten oxides of the tetragonal tungsten bronze type [J]. Acta Crystallographica Section B, 1999, B54: 240−249.

[17] FRANK K, HUTCHISON J L, SAYAGUEAS M J. In-situ oxidation products of $Nb_4W_{13}O_{47}$: A high-resolution transmission electron microscopy study [J]. Zeitschrift Für Anorganische Und Allgemeine Chemie, 1999, 625: 755−763.

[18] FRANK K, GRORG L, WERNER M. A novel intergrowth structure between ReO_3-type and tetragonal tungsten bronze-type in the Zr/Nb/W/O system [J]. Acta Crystallographica, 1996, B52: 917−922.
[19] GRIFFITH K J, WIADEREK K M, CIBIN G, MARBELLA L E, GREY C P. Niobium tungsten oxides for high-rate lithium-ion energy storage [J]. Nature, 2018, 559: 556−563.
[20] LIU Wei-wei, XU Meng, ZHU Meng-hua. Design of niobium tungsten oxide/C micro-structured electrode for fast charging lithium-ion batteries [J]. Inorganic Chemistry Frontiers, 2021, 8: 1−13.
[21] ROTH R S, WADSLEY A D. Multiple phase formation in the binary system Nb_2O_5−WO_3. I: Preparation and identification of phases [J]. Acta Crystallographica, 1965, 19: 26−32.
[22] PERDEW J P, BURKE K, ERNZERHOF M. Generalized gradient approximation made simple [J]. Physical Review Letters, 1996, 77: 3865−3868.
[23] HAMMER B, HANSEN L B, NORSKOV J K. Improved adsorption energetics within density-functional theory using revised Perdew-Burke-Ernzerhof functionals [J]. Physical Review B, 1999, 59: 7413−7421.
[24] BLOCHL P E. Projector augmented-wave method [J]. Physical Review B, 1994, 50: 17953−17979.
[25] KRESSE G, JOUBERT D. From ultrasoft pseudopotentials to the projector augmented-wave method [J]. Physical Review B, 1999, 59: 1758−1775.
[26] CHADI D J. Special points for Brillouin-zone integrations [J]. Physical Review B, 1977, 16: 1746−1747.
[27] HENKELMAN G, JONSSON H. Improved tangent estimate in the nudged elastic band method for finding minimum energy paths and saddle points [J]. The Journal of Chemical Physics, 2000, 113: 9978−9985.
[28] HENKELMAN G, UBERUAGA B P, JONSSON H. A climbing image nudged elastic band method for finding saddle points and minimum energy paths [J]. The Journal of Chemical Physics, 2000, 113: 9901−9904.
[29] SHEPPARD D, HENKELMAN G. Paths to which the nudged elastic band converges [J]. Journal of Computational Chemistry, 2011, 32: 1769−1771.
[30] ZHANG Jia-yong, ZHANG Hong-wu, YE Hong-fei, ZHENG Yong-gang. Free-end adaptive nudged elastic band method for locating transition states in minimum energy path calculation [J]. Journal of Chemical Physics 2016, 145: 1−9.

四方钨青铜(TTB)相 $Nb_{18}W_{16}O_{93}$ 材料的锂离子扩散路径

沈 超[1,2]，姜赛男[1]，丁翠敏[1]，薛伟顺[3]，谢科予[1,2]

1. 西北工业大学 材料科学与工程学院 纳米能源材料研究中心，凝固国家技术重点实验室，西安 710072；
2. 西北工业大学 深圳研究生院，深圳 518057；
3. 中国电子科技集团公司第十八研究所，天津 300384

摘 要：使用改进的固态烧结方法(1000 ℃，36 h)成功合成四方钨青铜(TTB)相 $Nb_{18}W_{16}O_{93}$，并通过 XRD，SEM 和 XPS 对其进行表征与分析。GITT 结果表明，$Nb_{18}W_{16}O_{93}$($10^{-12}cm^2/s$)的锂离子扩散系数高于传统的 Ti 基负极。使用密度泛函理论模拟计算揭示锂离子的扩散机制。TTB 相有 3 种扩散路径，其中扩散能垒最小的层间扩散(0.46 eV)比其他典型负极(例如，石墨 0.56 eV)更具有优势，使 TTB 相 $Nb_{18}W_{16}O_{93}$ 成为潜在的高特定功率阳极材料。

关键词：锂离子电池；铌钨氧化物；四方钨青铜相；锂离子扩散机制；扩散路径

(Edited by Bing YANG)